J. Fluid Mech. (1978), *vol.* 85, *part* 2, *pp.* 305-323
Printed in Great Britain

Numerical simulation of helical magnetohydrodynamic turbulence

By A. POUQUET† AND G. S. PATTERSON
National Center for Atmospheric Research, Boulder, Colorado 80303

(Received 19 April 1976 and in revised form 23 May 1977)

The three-dimensional incompressible magnetohydrodynamic (MHD) equations for rectangular geometry and periodic boundary conditions are solved numerically using the spectral method of Orszag & Patterson (1972). The calculations are restricted to a magnetic Prandtl number of one and to Gaussian random initial conditions with zero mean magnetic and momentum fields. We permit non-mirror-symmetric (helical) flows. In all cases, there is a continuous transfer of energy from the momentum field to the magnetic field. A proposed mechanism for this transfer involves the cascading of energy from the large scales of the momentum field to the small scales, thence a redistribution of energy between the momentum and magnetic fields by Alfvén waves, and, finally, an inverse cascade of energy from the small scales of the magnetic field to the large scales. This inverse cascade is found when magnetic helicity ($\langle \mathbf{a} . \mathbf{b} \rangle$, where $\mathbf{b} = \operatorname{curl} \mathbf{a}$ is the magnetic induction) is present in the flow.

1. Introduction

In this paper, we present the results of a numerical simulation of homogeneous MHD turbulence. These flows are three-dimensional, incompressible, isotropic, and include non-mirror-symmetric (helical) realizations. For the sake of simplicity in analysing the results, no forcing terms were included in the calculations reported in this paper. Since both the kinetic and the magnetic energy eventually disappears through dissipative processes, no steady state can be reached. Reynolds numbers attained in these direct numerical simulations were restricted to moderate values because of limited available computing power. However, overall features of the dynamics of MHD turbulence can be demonstrated, in particular the mechanisms for transforming kinetic into magnetic energy. These mechanisms include equipartition in the small scales, and the amplification of large-scale magnetic energy when magnetic helicity is initially present in the flow.

These studies are motivated by the magnetic-dynamo problem, in which a mechanism is sought whereby a momentum field can sustain a large-scale magnetic field. Since the extension of these numerical simulations to non-rectangular geometries and to rotating frames of reference is difficult, we cannot explicitly simulate a magnetic dynamo. Forcing terms can be added to the momentum equation, but they are necessarily artificial, and it is important to understand the unforced case first. The addition of forcing does permit a calculation to proceed for times long compared with the Ohmic dissipation times of the large scales in the flow. Forcing studies are in progress and will

† Permanent address: Observatoire de Nice, Nice, France 06300.

be reported on in another paper. Nevertheless, significant insight into the energy transfer mechanisms can be obtained from decaying turbulent flows and by using initial random fields with non-mirror-symmetric statistical properties to mimic the effects of rotation. These energy transfer mechanisms are of interest in gaining insight into the magnetic-dynamo problem as well as into other turbulent MHD flows.

Numerical calculations of the full MHD equations have not been carried out. Thomas (1968) made a numerical integration of a one-dimensional model of the MHD equations (analogous to Burgers' equation). Moss (1970) did a kinematic two-dimensional calculation. Bullard & Gellman (1954) opened the way to three-dimensional calculations by taking a conducting sphere and expanding both the velocity and the magnetic field in spherical harmonics. Their calculations were kinematic (fluid velocity specified) and there were questions of convergence as additional harmonics were included. Jepps (1975) has recently carried out a kinematic calculation of a modified magnetic induction equation in a sphere. The nonlinear problem has been attempted (Stevenson & Wolfson 1966; Kropachev 1971*a*, *b*). Gubbins (summarized in Gubbins 1974) has recently extended Bullard & Gellman's method. He integrates the induction equation together with the equation of motion, neglecting the inertial term but keeping the Lorentz force. Schumann (1975) has done direct numerical simulations of a very large magnetic Prandtl number turbulent flow with the Lorentz force represented by a linear functional of the momentum field and using a modified Orszag–Patterson (1972) code.

Besides these numerical studies, the fully nonlinear turbulent MHD equations have been studied theoretically over the past several years, and this has led to the introduction of some important ideas. They are summarized in the following section.

2. The turbulent MHD equations

When the displacement current in Maxwell's equations is neglected (non-relativistic case), the MHD equations for an incompressible fluid may be written in the following form:

$$\partial \mathbf{u}/\partial t - \nu \nabla^2 \mathbf{u} = (\mathbf{u} \times \boldsymbol{\omega}) + (\mathbf{j} \times \mathbf{b}) - \nabla P, \tag{1a}$$

$$\partial \mathbf{b}/\partial t - \lambda \nabla^2 \mathbf{b} = \operatorname{curl}(\mathbf{u} \times \mathbf{b}), \tag{1b}$$

$$P = p/\rho + \tfrac{1}{2}\mathbf{u}.\mathbf{u}, \tag{1c}$$

$$\boldsymbol{\omega} = \operatorname{curl} \mathbf{u}, \quad \mathbf{j} = \operatorname{curl} \mathbf{b} \tag{1d,e}$$

and

$$\operatorname{div} \mathbf{u} = \operatorname{div} \mathbf{b} = 0, \tag{1f}$$

where $\mathbf{u} = \mathbf{u}(\mathbf{x}, t)$ is the velocity field and $\mathbf{b} = \mathbf{b}(\mathbf{x}, t)$ is the magnetic induction field normalized by $(\rho\mu_0)^{\frac{1}{2}}$. $\boldsymbol{\omega}$ is the vorticity field, $\mathbf{j}$ the normalized electric current and P the normalized pressure. The physical parameters are the density ρ, the permeability μ_0, the kinematic viscosity ν and the magnetic diffusivity $\lambda = 1/\sigma\mu_0$, with σ the electrical conductivity.

No forcing terms are included and (1*a–f*) refer to a non-rotating frame of reference. For these experiments, the magnetic Prandtl number $Pr_M = \nu/\lambda$ was taken to be equal to 1. Boundary conditions were periodic on a cube of side L (this represents a flow in an infinite domain with maximum resolvable scale L). Initial conditions were random with Gaussian statistics and are described further in the appendix.

In the absence of a magnetic field, kinetic energy is transferred from the larger scales of the flow to the smaller dissipative scales via what appears to be a complicated cascade process. The term 'cascade' refers to transfer across a range of scales where interactions are repeated between progressively smaller scales of motion. In the presence of a magnetic field, this cascade process appears to continue to occur with additional energy transfer from small scales of the velocity field to small scales of the magnetic field through the action of Alfvén waves. These waves (Roberts 1967) are non-dispersive, transverse and act to partition energy between the momentum and magnetic fields with a characteristic time $1/kE_M^{\frac{1}{2}}$, where k is the wavenumber and E_M the total magnetic energy. Because of the k dependence, this energy equipartition is more effective at the smaller scales (large k) of the motion.

Together with energy transfer into the smaller scales of the magnetic field by Alfvén waves, it is thought that an *inverse* transfer will persistently shift energy into the larger scales (see, for example, Léorat 1975). These scales have relatively long characteristic times. By this circuitous process, the magnetic field may be supported by the momentum field.

The concept of an inverse cascade of energy is well established from studies of two-dimensional turbulence. The presence of two quadratic invariants of motion (in the absence of viscosity), kinetic energy and squared vorticity, constrains the motion sufficiently so that the normal cascade process is reversed. In MHD turbulence, this inverse cascade appears to be related to non-mirror-symmetric flows. Kinetic helicity ($\langle \mathbf{u}.\boldsymbol{\omega} \rangle$, angle brackets denoting a volume average over the cube) can be non-zero in isotropic turbulence if the requirement for mirror symmetry is relaxed. Moreover, in the absence of a magnetic field, it is an invariant of the inviscid motion.

The presence of kinetic helicity is important in Steenbeck, Krause & Rädler's (1966) explanation of a means of generating a turbulent magnetic field (the α-effect). Briefly,

$$\langle \mathbf{u}.\mathbf{b} \rangle_{\substack{\text{small} \\ \text{scales}}} \simeq \alpha_V \langle \mathbf{b} \rangle_{\substack{\text{large} \\ \text{scales}}}, \tag{2}$$

where $\alpha_V = -\frac{1}{3}\tau\langle \mathbf{u}.\boldsymbol{\omega} \rangle$ and τ is an Eulerian integral time scale.

Moffatt (1970*a*) has proposed a similar mechanism, but with α_V a more general functional of the helicity. In both these studies, contrary to the present one, the magnetic field is inhomogeneous. But it is felt that the α-effect is also applicable to homogeneous fields. The source of kinetic helicity is not well established, but presumably it may come from either a rotation effect or from density gradients, or both. A mechanism that will impart a right-handedness or left-handedness to the flow will suffice.

The linearizations done by Steenbeck *et al.* and Moffatt lead to an exponential growth of the magnetic field. This process is halted by the Lorentz force $\mathbf{j} \times \mathbf{b}$ acting on the momentum field. The saturation mechanism is often thought to be an enhanced Ohmic dissipation (Weiss 1966; Moffatt 1970*b*, 1972; Malkus & Proctor 1975). In the last paper, for example, it is assumed that the characteristic time of the problem is the Ohmic decay time $1/\lambda k^2$, and that the Lorentz force induces a large-scale velocity field which, in turn, bends the magnetic field lines, hence creating small scales in the magnetic field which will be readily dissipated. Moffatt envisages that the velocity field, which is the source of the magnetic field, is dissipated and he is able to show explicitly how the α-effect may be diminished by the introduction of the Lorentz force. Indeed,

an expression of the form $\alpha = \alpha_V - \alpha_M$ has been suggested by several authors as a means of saturating the magnetic field (Rüdiger 1973; Vainshtein & Zeldovich 1972; Vainshtein & Vainshtein 1973; Stix 1972; Malkus & Proctor 1975). Vainshtein (1974) was interested in the contribution of the Lorentz force to the creation of kinetic helicity. By assuming a form of the correlation tensor of the velocity field depending upon the magnetic field, and by assuming further a weak-field regime, he was able to show that the contribution of the Lorentz force is proportional to

$$\alpha_M \cong -\tfrac{1}{3}\tau\langle \mathbf{b}.\mathbf{j}\rangle \tag{3}$$

and that it acts in an opposite manner to the kinetic helicity. Therefore, the total growth factor $\alpha = \alpha_V - \alpha_M$ of the magnetic field is reduced. However, this analysis is restricted to weak fields, so that the magnetic energy remains smaller at all times than the kinetic energy.

Homogeneous incompressible turbulent flows have been productively studied using stochastic models and some closure approximation (Leslie 1973).† These models have been checked against experiments (Herring 1973) and against numerical simulations in two and three dimensions (Herring *et al.* 1974; Orszag & Patterson 1972). Such models exist for MHD turbulence (Kraichnan 1958) and studies have been made of realizable, incompressible, isotropic and homogeneous conducting flows (Kraichnan & Nagarajan 1967; Nagarajan 1971). Also, turbulence which is isotropic but not mirror symmetric has been investigated recently (Kraichnan 1973; Patterson 1973; Léorat 1975; Pouquet, Frisch & Léorat 1976). Léorat shows that the fluctuating magnetic energy grows when there is some residual helicity $\langle \mathbf{u}.\boldsymbol{\omega}\rangle - \langle \mathbf{b}.\mathbf{j}\rangle$ available in the smaller scales. As the Alfvén waves reduce the value of the residual helicity in time, this provides an equilibration mechanism, although the ultimate fate of the magnetic energy is not clear (Pouquet *et al.* 1976).

3. Direct spectral simulations of the MHD equations

With periodic boundary conditions at the surfaces of a cube of side L, the velocity field (for example) may be expanded in a Fourier series

$$\mathbf{u}(\mathbf{x}, t) = \sum_{\text{all } \mathbf{k}} \hat{\mathbf{u}}(\mathbf{k}, t) \exp(i\mathbf{k}.\mathbf{x}), \tag{4}$$

where $\mathbf{k} = (2\pi/L)\mathbf{n}$ with $-\frac{1}{2}N \leqslant n_i < \frac{1}{2}N$ $(i = 1, 2, 3)$, the n_i being integers and N^3 $(= 32^3)$ the number of points treated in real space. Defining the fields

$$\mathbf{s} = \mathbf{u}\times\boldsymbol{\omega} + \mathbf{j}\times\mathbf{b}, \quad \mathbf{z} = \mathbf{u}\times\mathbf{b} \tag{5}$$

and substituting (4) and equivalent expansions into (1), we arrive at

$$d\hat{\mathbf{u}}(\mathbf{k}, t)/dt + \nu k^2\hat{\mathbf{u}}(\mathbf{k}, t) = -k^{-2}\{\mathbf{k}\times[\mathbf{k}\times\hat{\mathbf{s}}(\mathbf{k}, t)]\}, \tag{6a}$$

$$d\hat{\mathbf{b}}(k, t)/dt + \lambda k^2\hat{\mathbf{b}}(\mathbf{k}, t) = i[\mathbf{k}\times\hat{\mathbf{z}}(\mathbf{k}, t)], \tag{6b}$$

$$\hat{\boldsymbol{\omega}} = i(\mathbf{k}\times\hat{\mathbf{u}}), \quad \hat{\mathbf{j}} = i(\mathbf{k}\times\hat{\mathbf{b}}), \quad \mathbf{k}.\hat{\mathbf{u}} = \mathbf{k}.\hat{\mathbf{b}} = 0. \tag{6c, d, e}$$

† The quadratic nonlinearity of the Navier–Stokes equations implies that the equation for the mean value of the velocity field depends upon second-order moments, which in turn are a function of third-order moments, etc. Therefore the set of equations for the moments of the velocity field is not closed and an additional hypothesis is necessary to give a finite system.

The pressure term has been removed by twice taking the curl of the momentum equation. $\hat{\mathbf{s}}$ and $\hat{\mathbf{z}}$ are computed in real space after transforming $\hat{\mathbf{u}}$, $\hat{\boldsymbol{\omega}}$, $\hat{\mathbf{b}}$ and $\hat{\mathbf{j}}$ from $\mathbf{k}$ space to real space [equation (5)], and then it is possible to step forward by means of (6). The time-differencing scheme used is a 'leapfrog' scheme with the linear terms handled implicitly.

The code used is a modification of that first described by Orzsag & Patterson (1972) for the integration of the Navier–Stokes equations. Because of the Alfvén waves, the time step had to be reduced from its value in the hydrodynamic code, and to conserve computer time (the code requires 6 s of CDC 7600 time per step), errors induced by aliasing interactions were not removed. However, a truncation in wavenumber space was effected which eliminates even-order aliasing interactions (Patterson & Orszag 1971). Tests indicated that these errors were negligible and less than time-stepping errors, which were small compared with truncation errors (discussed below).

Statistical averages for spectra are obtained by summing over spherical shells in wavenumber space. A sum over those shells is equivalent to a volume average over the cube.

We define an energy spectrum $\hat{E}(k,t)$, an enstrophy spectrum $\hat{D}(k,t)$ and a transfer spectrum $\hat{T}(k,t)$ as follows:

$$\left.\begin{matrix}\hat{E}_V(k,t)\\ \hat{D}_V(k,t)\\ \hat{T}_V(k,t)\\ \hat{E}_M(k,t)\\ \hat{D}_M(k,t)\\ \hat{T}_M(k,t)\end{matrix}\right\} = \sum_{k-\Delta k\leqslant|\mathbf{k}'|<k+\Delta k} \begin{cases}\hat{u}_i(\mathbf{k}',t)\,\hat{u}_i(-\mathbf{k}',t), & (7a)\\ \hat{\omega}_i(\mathbf{k}',t)\,\hat{\omega}_i(-\mathbf{k}',t), & (7b)\\ \frac{1}{2}[\hat{u}_i(\mathbf{k}',t)\,\hat{t}_i(-\mathbf{k}',t)+\hat{u}_i(-\mathbf{k}',t)\,\hat{t}_i(\mathbf{k}',t)], & (7c)\\ \hat{b}_i(\mathbf{k}',t)\,\hat{b}_i(-\mathbf{k}',t), & (7d)\\ \hat{j}_i(\mathbf{k}',t)\hat{j}_i(-\mathbf{k}',t), & (7e)\\ \frac{1}{2}[\hat{b}_i(\mathbf{k}',t)\,\hat{y}_i(-\mathbf{k}',t)+\hat{b}_i(-\mathbf{k}',t)\,\hat{y}_i(\mathbf{k}',t), & (7f)\end{cases}$$

where $\hat{\mathbf{t}} = -k^{-2}[\mathbf{k}\times(\mathbf{k}\times\hat{\mathbf{s}})]$ and $\hat{\mathbf{y}} = i(\mathbf{k}\times\hat{\mathbf{z}})$. By forming moments of (6) and shell averaging, we obtain

$$\frac{1}{2}\frac{d\hat{E}_V}{dt}+\nu\hat{D}_V=\hat{T}_V, \quad \frac{1}{2}\frac{d\hat{E}_M}{dt}+\lambda\hat{D}_M=\hat{T}_M. \tag{8}$$

Summing over all shells, we get

$$E_V(t)=\sum_{\text{all }k}\hat{E}_V(k,t), \tag{9}$$

and similarly for the other variables. If $\nu=\lambda=0$, the total energy E_V+E_M is conserved, i.e.

$$\sum_{\text{all }k}[\hat{T}_V(k,t)+\hat{T}_M(k,t)]=0. \tag{10}$$

Other quadratic invariants (conserved quantities in an inviscid, non-diffusive flow) are the magnetic helicity $H_M(t)$ and the cross-helicity $H_C(t)$, defined below. When the magnetic field is absent, the kinetic helicity $H_V(t)$ is an invariant. Here

$$\left.\begin{matrix}H_V(t)\\ H_M(t)\\ H_C(t)\end{matrix}\right\} = \sum_{\text{all }k}\begin{cases}\hat{H}_V(k,t), & (11a)\\ \hat{H}_M(k,t), & (11b)\\ \hat{H}_C(k,t), & (11c)\end{cases}$$

where
$$\left.\begin{matrix}\hat{H}_V(k,t)\\ \hat{H}_M(k,t)\\ \hat{H}_C(k,t)\end{matrix}\right\} = \sum_{k-\Delta k\leqslant|\mathbf{k}'|<k+\Delta k} \begin{cases}\hat{u}_i(\mathbf{k}',t)\,\hat{\omega}_i(-\mathbf{k}',t), & (12a)\\ k^{-2}[\hat{b}_i(\mathbf{k}',t)\hat{j}_i(-\mathbf{k}',t)], & (12b)\\ \hat{u}_i(\mathbf{k}',t)\,\hat{b}_i(-\mathbf{k}',t). & (12c)\end{cases}$$

In real space
$$H_V(t) = \langle \mathbf{u}.\boldsymbol{\omega}\rangle, \quad (13a)$$
$$H_M(t) = \langle \mathbf{b}.\mathbf{a}\rangle, \quad \mathbf{b} = \operatorname{curl}\mathbf{a}, \quad (13b)$$
and
$$H_C(t) = \langle \mathbf{u}.\mathbf{b}\rangle. \quad (13c)$$

Relative kinetic, magnetic and cross-helicities are defined as

$$\eta_V(k,t) = \frac{\hat{H}_V(k,t)}{k\hat{E}_V(k,t)}, \quad \eta_M(k,t) = \frac{\hat{H}_M}{\hat{E}_M(k,t)/k}, \quad (14a,b)$$

$$\eta_C(k,t) = \frac{\hat{H}_C(k,t)}{[\hat{E}_V(k,t)\,\hat{E}_M(k,t)]^{\frac{1}{2}}}, \quad (14c)$$

respectively, and their absolute values are bounded by unity (see Frisch *et al.* 1975). Any helicity is said to be maximal at a given wavenumber if the corresponding relative helicity for that wavenumber is equal to ± 1.

Pertinent physical and computational parameters of the flow are summarized in table 1. A summary of calculations reported here is given in table 2. (The variable $\psi(t)$ is the ratio of magnetic energy $E_M(t)$ to kinetic energy $E_V(t)$.) An algorithm for generating helical fields is given in the appendix.

4. Numerical results

Growth of the magnetic energy

In this study, emphasis is placed upon the nonlinear problem, i.e. when $\langle u^2\rangle \sim \langle b^2\rangle$, and we shall look at the effect of a magnetic field upon the turbulent characteristics of the flow, and vice versa. We started our calculations with a case where the initial ratio of magnetic to kinetic energy, denoted by

$$\psi(t) = E_M(t)/E_V(t), \quad (15)$$

was 10^{-2}. For run 1(*c*) (refer to table 2), $\psi(t)$ grows monotonically to a value of 7 by $t = 1{\cdot}5$, mainly because of the fast equipartition of kinetic and magnetic energies at large wavenumbers owing to Alfvén waves. Similar, but slightly lower, values are observed for runs 3(*b*) and (*a*). Almost no magnetic energy is gained in the first shell, but the transfer at larger wavenumbers is rapid. In fact, there is a definite overshoot of the magnetic energy for large k, and this is observed in almost all runs which have been tried (table 2). Kinetic and magnetic energy spectra for run 1(*b*) are presented in figure 1.

Even when initially the kinetic and magnetic energy are equal ($\psi(0) = 1$), the ratio $\psi(t)$ increases with time. Figure 2 shows this ratio for runs 3(*a*)–(*g*). For runs 3(*c*) and (*d*), both of which have maximal magnetic helicity initially ($\eta_M(k,0) = 1$), the overshoot of magnetic energy is more important than in the other cases. This can be attributed to a strong correlation between the current and the magnetic field (their Fourier components are nearly parallel), which noticeably reduces the Lorentz force.

$Pr_M = \nu/\lambda$	magnetic Prandtl number	1
ν	kinematic viscosity	0·01
k_0	wavenumber of energy peak at $t = 0$	4·76
$k_{\min} = 2\pi/L$	minimum wavenumber of calculation	2
$k_{\max}$	maximum wavenumber of calculation	31
u_0	r.m.s. velocity at $t = 0$	1
Δt	time increment	0·002
Re_λ $(t = 0)$	Reynolds number (based on Taylor microscale)	40
$t_{\max}$	maximum time	$\geqslant 0{\cdot}8$
Characteristic times:		
Alfvén time $1/k_{\max}b_0$		0·03 (if $b_0 = u_0$)
Dissipation time $1/\nu k_{\max}^2$		0·1
Eddy turnover time $1/k_{\min}u_0$		0·5

TABLE 1

Run	Identification	$\eta_V(k, 0)$	$\eta_M(k, 0)$	$\eta_C(k, 0)$	$\psi(0)$	$\psi(0{\cdot}8)$	$t_{\max}$
1 (*a*)†	N50	—	—	—	10^{-2}	$5{\cdot}5 \times 10^{-2}$	1·5
1 (*b*)	N51	1	—	—		$6{\cdot}5 \times 10^{-2}$	1·5
1 (*c*)	N52	—	1	—		$7{\cdot}0 \times 10^{-2}$	1·5
2 (*a*)	N70	—	—	—	0·2	0·65	0·8
2 (*b*)	N71	1	—	—		0·57	0·8
2 (*c*)‡	N72	—	1	—		1·25	0·8
3 (*a*)	N53	—	—	—	1	1·38	0·8
3 (*b*)	N54	1	—	—		1·18	0·8
3 (*c*)§	N55	—	1	—		3·25	1·5
3 (*d*)¶	N60	1	1	—		3·22	3
3 (*e*)	N80	−1	1 if $2 \leqslant k < 4$; 0 otherwise	—		3·45	0·8
3 (*f*)	N63	—	—	0·5		1·16	0·8
3 (*g*)	N86	—	1	0·5		2·54	0·8

† All helicities are initially zero unless otherwise specified.
‡ Additional runs with $\nu = 0{\cdot}02$, 0·03 and 0·04 and varying $k_{\min}$ and Δt.
§ Additional run with $k_0 = 6{\cdot}5$.
¶ Additional runs with $\nu = 0$ and with aliasing removed.

TABLE 2

However, the condition of maximal helicity is not conserved by the equations of motion (Kraichnan 1973), and soon the almost force-free condition is relaxed. Run 3 (*d*) was continued until $t = 3$ but no saturation appeared, although only 15 % of the initial energy was left. It should be emphasized that the growth of $\psi(t)$ does not, in general, represent an actual increase in the total magnetic energy above its initial value, but only an increase over the total kinetic energy at that time. In other words, we cannot say that we are dealing with a dynamo because no source of energy is present that would keep the total energy steady; nevertheless, the results presented in this paper give a clear indication of the mechanisms of energy transfer and the magnitude of that transfer when all terms in the equations are retained, and no linearization is permitted.

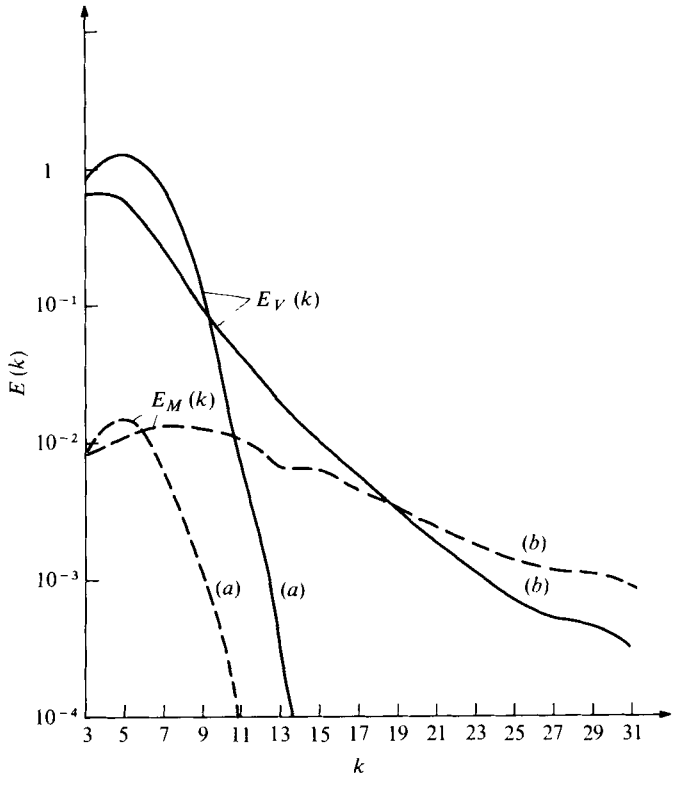

FIGURE 1. Kinetic (solid lines) and magnetic (dashed lines) energy spectra for run 1 (*b*) at (*a*) time $t = 0$ and (*b*) $t = 3$.

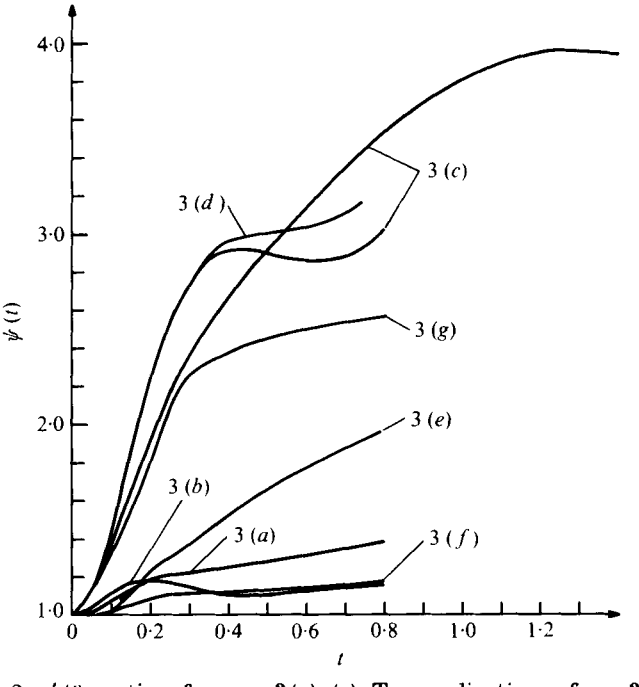

FIGURE 2. $\psi(t)$ *vs.* time for runs 3 (*a*)–(*g*). Two realizations of run 3 (*c*) are shown.

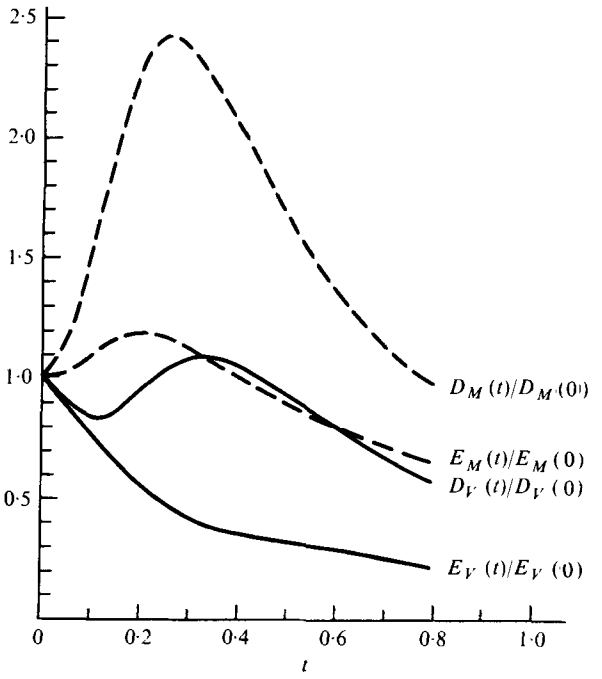

FIGURE 3. Kinetic (solid lines) and magnetic (dashed lines) energies and enstrophies *vs.* time for run 3 (*c*). All quantities are normalized by their initial values.

The variation of ψ with time is linked to the magnetic Reynolds number of the flow. By increasing the viscosity (and the magnetic diffusivity since $Pr_M = 1$), but otherwise keeping the same initial conditions, we can establish the following empirical relationship:

$$\psi \sim \nu^{-0.4}. \tag{16}$$

The stretching of the magnetic field lines is the cause of the increase in the magnetic energy over the kinetic energy in the small scales. With a lower magnetic Reynolds number, less stretching, and therefore less growth, occurs. This stretching effect can be further seen in figure 3, where the total kinetic enstrophy D_V and its magnetic counterpart D_M are drawn *vs.* time. The magnetic enstrophy clearly grows more than the kinetic enstrophy. The most dramatic increase in D_M occurred in runs 1 (*b*) and (*c*), where it was over 18 times its initial value. D_V increased by a factor of 1·2, which is similar to that observed in calculations with the Navier–Stokes equations (see Orszag & Patterson 1972). This is expected for a weak magnetic field.

We can say that, as well as the turbulent transfer of energy to high wavenumbers as indicated by D_V, there is also observed another kind of transfer, due to the Alfvén waves. This type of transfer is particularly strong when the initial value of the residual energy (and helicity) is far from zero, as in the series 1 runs. In fact, if we define the transfer function for the kinetic energy as the sum of contributions from the $\mathbf{u} \times \boldsymbol{\omega}$ term and the $\mathbf{j} \times \mathbf{b}$ term [(5), (7) and (9)], i.e.

$$T_V(t) = T_V^{NS}(t) + T_V^{L}(t), \tag{17}$$

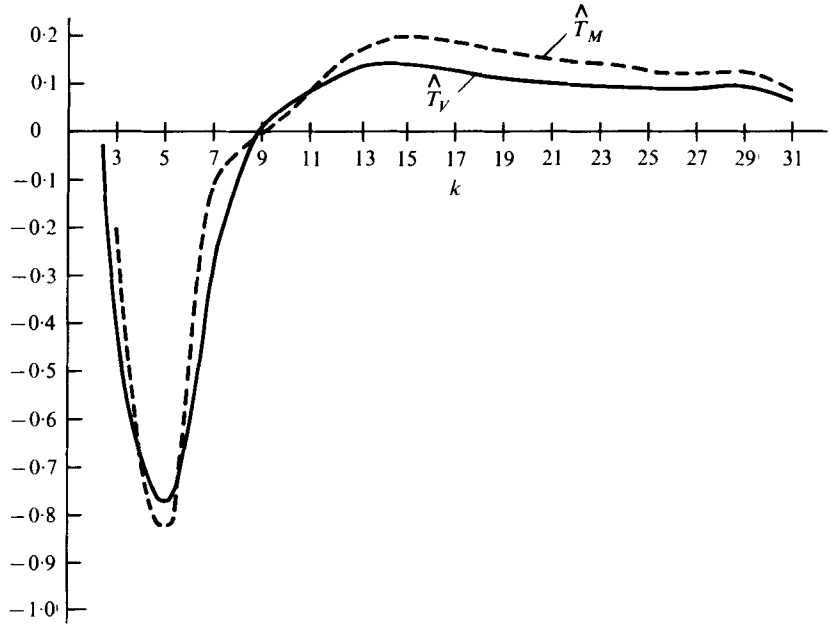

FIGURE 4. Kinetic (solid line) and magnetic (dashed line) energy transfer spectra at time $t = 0{\cdot}3$ for run 3 (a).

we find that the transfer term $T_V^L(t)$ due to the Lorentz force is negative. This indicates a systematic feeding of kinetic energy into magnetic energy. Transfer spectra are shown in figure 4; energy is removed from large-scale eddies and transferred to small-scale eddies, presumably by a cascade process. The low Reynolds number of the calculation does not allow for any significant inertial range, and we are not able, so far, to verify the theoretical prediction of Kraichnan (1965) of a $k^{-\frac{3}{2}}$ power law for kinetic and magnetic energy spectra in MHD turbulence. Figure 5 shows the normalized second-order moments of the transfer functions, defined as

$$S_V = \tfrac{5}{3}\tfrac{4}{5}[\lambda_V/\langle \mathbf{u}.\mathbf{u}\rangle]^3 \sum_{\text{all } k} k^2 \hat{T}_V(k,t), \tag{18a}$$

with

$$\lambda_V = [5\langle \mathbf{u}.\mathbf{u}\rangle/\langle \boldsymbol{\omega}.\boldsymbol{\omega}\rangle]^{\frac{1}{2}}, \tag{18b}$$

and similarly for S_M. For the Navier–Stokes equations, S_V reduces to the skewness factor

$$S = \left\langle \left(\frac{\partial u_1}{\partial x_1}\right)^3 \right\rangle \Big/ \left\langle \left(\frac{\partial u_1}{\partial x_1}\right)^2 \right\rangle^{\frac{3}{2}},$$

and λ_V is the Taylor microscale

$$\lambda = \langle u_1^2 \rangle \Big/ \left\langle \left(\frac{\partial u_1}{\partial x_1}\right)^2 \right\rangle^{\frac{1}{2}}. \tag{19}$$

These moments are a measure of the departure from Gaussianity, and indicate how transfer varies with time at high wavenumbers. They decrease substantially after having reached their sharp maximum and before stabilizing. It is possible that this is an indication of truncation errors, the energy being reflected back because it cannot be dissipated fast enough at high wavenumbers. Another indication of truncation is seen in the magnetic enstrophy spectrum (figure 6). We have checked that the observed

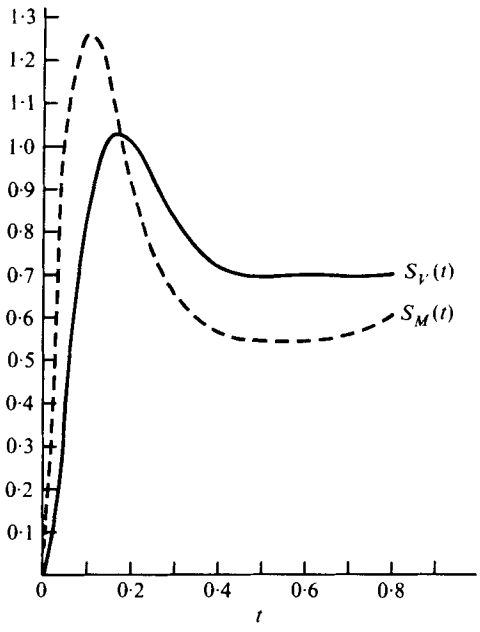

FIGURE 5. Kinetic (solid line) and magnetic (dashed line) skewnesses *vs.* time for run 3(*a*).

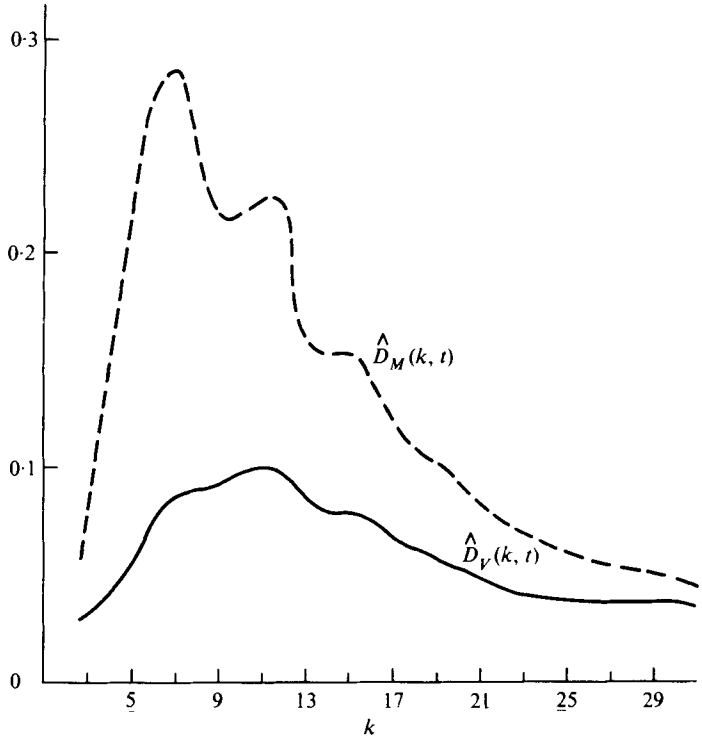

FIGURE 6. Kinetic (solid line) and magnetic (dashed line) enstrophy spectra at time $t = 0{\cdot}3$ for run 3(*c*).

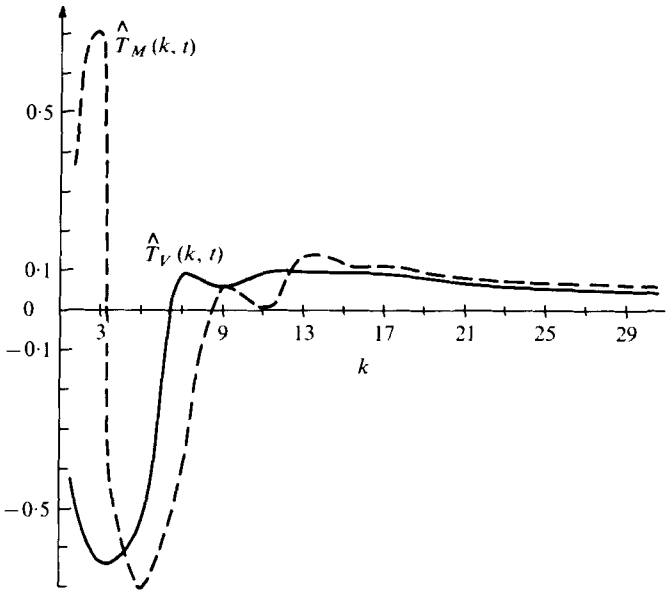

FIGURE 7. Kinetic (solid line) and magnetic (dashed line) energy transfer spectra at time $t = 0{\cdot}3$ for run 3(c).

oscillations are due neither to time-differencing errors nor to aliasing errors. A spurious effect due to the way statistics are handled might be partly the cause, because the number of points in each shell does not vary smoothly with k^2. However, when the viscosity is increased by a factor of four, the oscillations disappear. The kinetic enstrophy spectrum does not show these oscillations so markedly, partly because less transfer occurs for the kinetic energy than for the magnetic energy at high wavenumbers. In fact, such a non-monotone behaviour of the spectrum is present in Orszag & Patterson's calculations (1972, figure 2*a*). In any case, truncation errors are not so important as to cause the energy spectra to peak at the high wavenumbers; we were also able to check Reynolds number independence for the large scales.

Inverse transfer of the magnetic energy

The transfer spectra of magnetic energy and magnetic helicity behave differently when there is initially maximal magnetic helicity in the flow. In that case, both transfer spectra are positive in the first shell, indicating that an inverse transfer of magnetic energy (and magnetic helicity) is occurring towards low wavenumbers, i.e. the transfer of energy into the large-scale motion of the magnetic field (figures 7 and 8). Indeed, in figure 9 the magnetic energy is seen to grow at low wavenumbers between $t = 0{\cdot}3$ and $t = 0{\cdot}8$ despite the fact that this is a viscous decay calculation. We should note that such positive transfer has already been found in the numerical simulation of two-dimensional turbulence, where an inverse cascade of energy towards the large scales is expected (Herring *et al.* 1974). Such inverse transfer was not noted in the case (3*b*) with maximal kinetic helicity. In figures 10 and 11, we plot the ratios of the kinetic and magnetic energy in the first shell ($2 \leqslant k < 4$) at time t to their initial values. In figure 10, $\eta_V(k, 0) = 1$ and, in figure 11, $\eta_M(k, 0) = 1$. When there is magnetic helicity initially, the magnetic energy increases in the large scales. It must be stressed

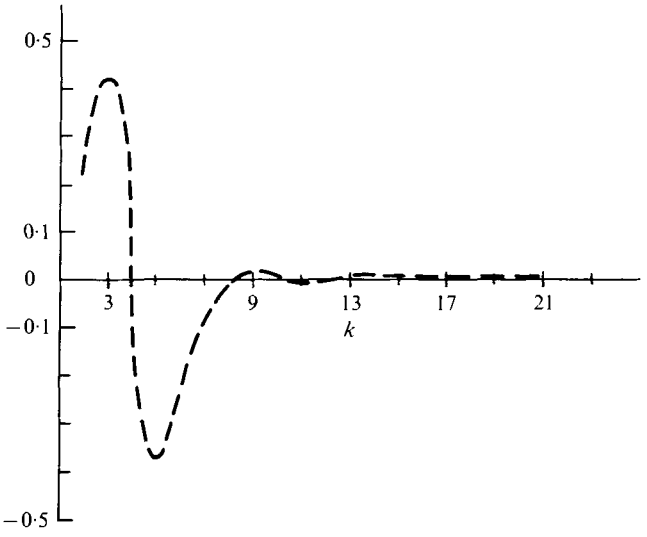

FIGURE 8. Magnetic helicity transfer spectrum at time $t = 0{\cdot}3$ for run 3(*c*).

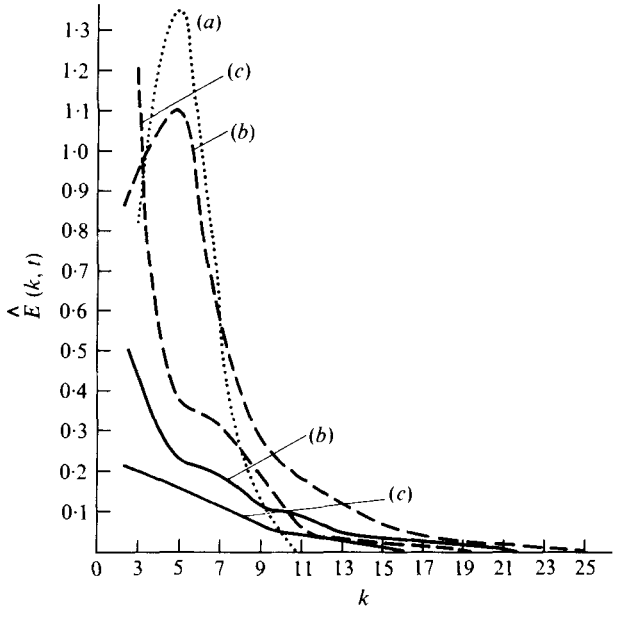

FIGURE 9. Kinetic (solid lines) and magnetic (dashed lines) energy spectra for run 3(*c*). (*a*) Initial spectrum ($\psi = 1$), (*b*) $t = 0{\cdot}3$, (*c*) $t = 0{\cdot}8$.

that it is the large-scale *fluctuating* energy which is growing, as there is *no mean* magnetic field in this problem. However, this result may have important consequences in astrophysics, because it demonstrates that turbulence is able to generate, under certain conditions, large-scale fluctuating fields such as those observed in the spiral arm of the Galaxy, for which $\Delta B \sim B$ (Parker 1969; Wilkinson & Smith 1976). The fact that no inverse transfer is found when only kinetic helicity is available in the flow seems to disagree with the results of previous studies of MHD. However, it was noted by Moffatt (1972) that the fastest growing mode of the magnetic field is the one for which

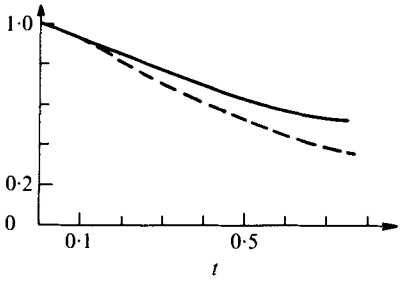

FIGURE 10. Normalized kinetic (solid line) and magnetic (dashed line) energy in the first shell ($k = 3$) *vs.* time for run 3(*b*).

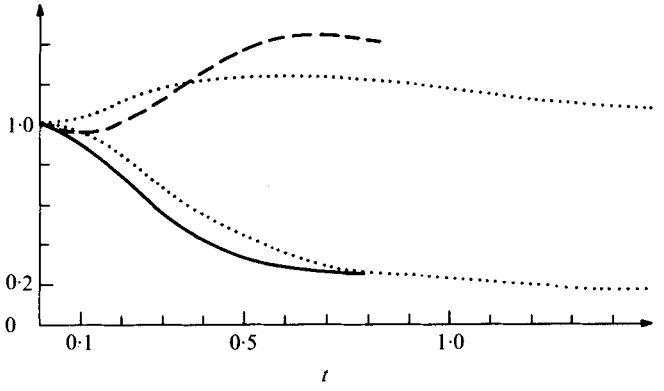

FIGURE 11. Normalized kinetic (solid line) and magnetic (dashed line) energy in the first shell ($k = 3$) *vs.* time for run 3(*c*). The dotted lines represent results for a different realization of the same case.

b is parallel to curl **b**, i.e. a field which possesses magnetic helicity. Also, in the work of Léorat, Frisch & Pouquet (1975), some large-scale magnetic helicity is necessary for growth of the large-scale magnetic energy. We therefore made run 3(*e*), which was similar to run 3(*b*) but with $\eta_V = -1$ and the magnetic helicity at a maximal rate in the first shell:

$$\eta_M(k, 0) = \begin{cases} 1, & 2 \leqslant k < 4, \quad (20a) \\ 0, & 4 \leqslant k < 32. \quad (20b) \end{cases}$$

The magnetic energy in the first shell does not decrease nearly as sharply as in the run 3(*b*) ($\eta_V = 1$, $\eta_M = 0$) although it is not seen to increase as in run 3(*c*) ($\eta_V = 0$, $\eta_M = 1$). Also, for this particular run 3(*e*), while the magnetic energy transfer is negative in the small wavenumbers, it is about half the value of the kinetic energy transfer. One can therefore say that there is some inverse (positive) transfer of magnetic energy but insufficient to overcome the usual negative component of transfer of energy towards large wavenumbers; the net magnetic energy transfer is still negative. The results are not as striking as for run 3(*c*), but they do not contradict the previously quoted papers as to the role of kinetic helicity in the dynamo problem for there the presence of magnetic helicity was also required.

A shift of the maxima of the initial energy spectra from the second ($k_0 = 4{\cdot}76$) shell to the third ($k_0 = 6{\cdot}5$) shell in a case otherwise identical to run 3(*c*) yields similar

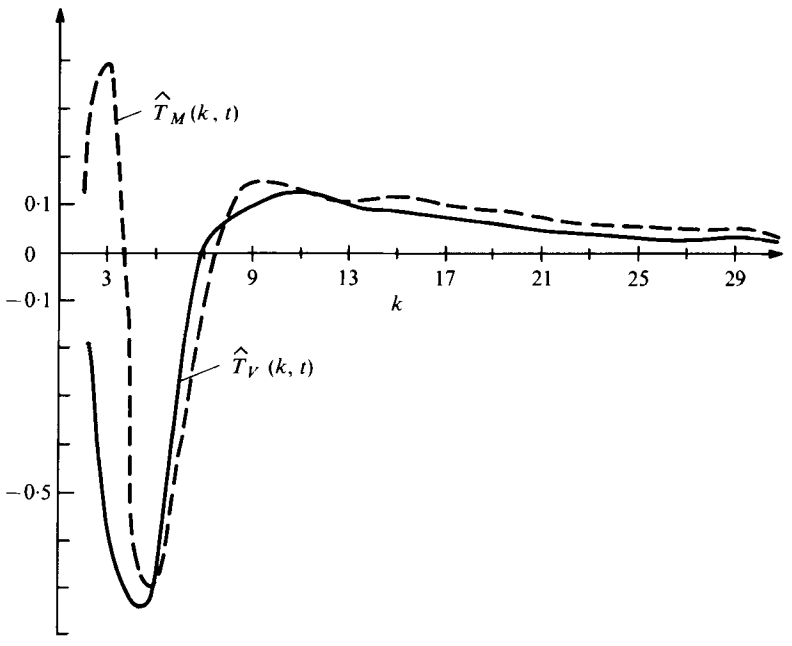

FIGURE 12. Kinetic (solid line) and magnetic (dashed line) energy transfer spectra at time $t = 0{\cdot}3$ for run 3(g).

results. As time increases, the kinetic energy stops diminishing in all scales except the largest and is found to increase again in a tendency towards equipartition. The remarkable feature here is that such an increase in the kinetic energy occurs in the second shell too, i.e. at a wavenumber smaller than the maximum of the initial spectrum (located in the third shell).

Cross-helicity

We finally studied the influence of the third invariant upon the development of the flow. The cross-helicity $\langle \mathbf{u} \cdot \mathbf{b} \rangle$ measures the correlation between the velocity field and the magnetic field. No model of MHD turbulence, to date, has included this invariant, except for the study of the inviscid case ($\nu = \lambda = 0$) by Frisch *et al.* (1975). If initially the kinetic and magnetic energies are equal and if the cross-helicity is maximal, all nonlinear terms are strongly reduced. For a non-maximal rate, it can therefore be expected that all transfers will be weakened. And in run 3(f), where $\psi(0) = 1$ and $\theta_C(k, 0) = 0{\cdot}5$, it is indeed observed that the dynamics are reduced and slowed down. The maxima for the enstrophies occur at a time ($t_M = 0{\cdot}35$) later than that when no cross-helicity is present ($t_M = 0{\cdot}30$), indicating a retardation of turbulent processes. Lesser transfer towards small scales is also indicated by a smaller increase in the ratio of magnetic to kinetic energy (a factor of 3 less than for the equivalent run without cross-helicity).

The weakening of turbulence in the presence of cross-helicity is further seen in run 3(g), for which the magnetic helicity is maximal. Again, we find an inverse transfer of magnetic energy (figure 12) and of magnetic helicity (figure 13). But the transfers are diminished from their values in the equivalent run without cross-helicity (run 3(c); compare figures 12 and 13 with figures 7 and 8). Furthermore, the cross-helicity itself

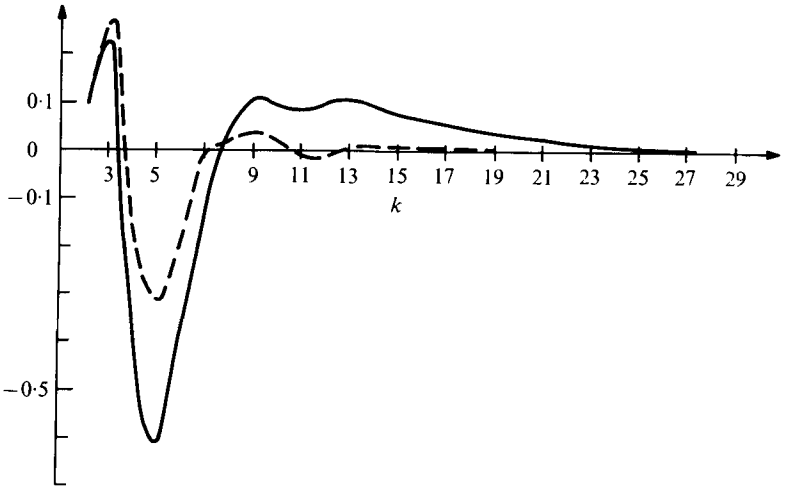

FIGURE 13. Cross (solid line) and magnetic (dashed line) helicity transfer spectra at time $t = 0{\cdot}3$ for run 3 (g).

is transferred to the large scales (figure 13). This inverse transfer indicates that the growth of the large-scale magnetic energy (and magnetic helicity) is accompanied by an amplification of the correlations between the large scales of the magnetic field and the velocity field.

Therefore, in the calculations presented in this paper, magnetic helicity appears to be the fundamental ingredient for the dynamo problem. We are not quite sure how these results would apply to the anisotrophic case. Indeed, in the presence of a mean magnetic field, the magnetic helicity invariant disappears and this is likely to have a direct influence on the dynamics of the flow.

5. Conclusion

This paper gives the results of a numerical simulation of isotropic but helical, homogeneous, incompressible, decaying, MHD turbulence at a magnetic Prandtl number of unity. The wavenumber range is approximately 15 (yielding a microscale Reynolds number of the order of 40), and the nonlinear terms are fully taken into account in the calculation. Statistical properties of the flow, such as non-mirror symmetry, can be included in the initial conditions. A net transfer of energy into the magnetic mode is seen to take place, first at high wavenumbers; this is attributed mainly to the equipartition action of the Alfvén waves. This transfer is more pronounced when there is helicity in the flow. In particular, when initially the magnetic helicity is maximal, an inverse transfer of magnetic energy and magnetic helicity is observed, feeding (over several eddy turnover times) the largest available scales of the flow. This inverse cascade of turbulent magnetic energy towards the large scales may possibly be relevant to the existence of large-scale magnetic fluctuations of the order of the mean field in our galaxy. Although the ultimate fate of the magnetic seed cannot be deduced from the computation because no source of energy is included, what appears clearly is that the nonlinear terms change the velocity field but do not diminish to a great extent the magnetic transfer term. These terms slow the growth

and eventually saturate it, but they do not eliminate it. A change in the value of the magnetic Prandtl number by an order of magnitude would modify the picture presented in this paper. However the computer code used does not permit the simulation of the wide range of scales that would be necessary.

Finally, it should be stressed that the numerical simulations are necessary for the validation of the closure models of turbulence, and are good tools, for that matter, as laboratory materials with a magnetic Prandtl number of unity do not exist. These closure models deal with equations bearing a structural relationship to the actual equations of MHD. They can be integrated numerically at high Reynolds number and they can be used with different values of the magnetic Prandtl number. Moreover, a detailed study of the dynamics of MHD is feasible in the framework of the models. In the absence of laboratory experiments at a magnetic Reynolds number of order one, there seems to be a need for numerical simulations of MHD turbulence in order to check the closure models against such calculations.

A. Pouquet wishes to thank NCAR for its generous hospitality. NCAR is sponsored by the National Science Foundation.

Appendix. Generation of initial velocity fields

The initial flow is chosen from a random Gaussian ensemble with a prescribed isotropic energy spectrum of the form

$$\hat{E}_V(k,0) \sim k^4 \exp\left[-2(k/k_0)^2\right]$$

with $k_0 = 4(2)^{\frac{1}{2}} \cong 4{\cdot}76$. $\hat{E}_V(k,t)$ is the kinetic energy in a spherical shell centred at wavenumber k and of thickness $2\Delta k = k_{\min} = 2$. Wavenumber space is restricted to a sphere that is partitioned into fifteen shells, and spectra are obtained by summing over all points within a shell. Statistical fluctuations are proportional to the number of points in a given shell, and are greater for the smaller wavenumbers. However, for some spectra, integral constraints imposed by conservation laws reduce these fluctuations. Statistical variations between two different realizations of the same flow are not significant. The total kinetic energy

$$\langle \mathbf{u}.\mathbf{u} \rangle = E_V(0) = \sum_{\text{all } k} \hat{E}_V(k,t)$$

is taken to be 3. The magnetic field is chosen similarly, with $E_M(0) = \psi(0) E_V(0)$ and $\psi(0)$ specified as 10^{-2}, 0·2 or 1.

The algorithm used to generate an initial random velocity field with a given kinetic helicity is as follows:

(*a*) Generate two random complex 3-vectors $\hat{\mathbf{q}}^{(1)}$ and $\hat{\mathbf{q}}^{(2)}$ which are normally distributed and all of whose components are independent, i.e.

$$\langle \mathbf{q}_i^{(\alpha)} \rangle = 0, \quad \langle \mathbf{q}_i^{(\alpha)} \mathbf{q}_j^{*(\alpha)} \rangle = 2\delta_{ij}, \tag{A 1}$$

where $\alpha = 1$ or 2, $i,j = 1,2$ or 3, the asterisk denotes complex conjugation and angle brackets denote an ensemble average.

(*b*) Generate two solenoidal complex 3-vectors with adjustable amplitude C:

$$\hat{\mathbf{v}}^{(\alpha)} = iC(n)\,(\mathbf{n} \times \hat{\mathbf{q}}^{(\alpha)}), \tag{A 2}$$

where $\mathbf{n} = \mathbf{k}/(2\pi/L)$ and $n = |\mathbf{n}|$.

(*c*) Correlate the two solenoidal complex 3-vectors:†

$$\begin{bmatrix}\hat{\mathbf{u}}^{(1)}\\ \hat{\mathbf{u}}^{(2)}\end{bmatrix} = \begin{bmatrix}\cos\theta\sin\theta\\ \sin\theta\cos\theta\end{bmatrix}\begin{bmatrix}\hat{\mathbf{v}}^{(1)}\\ \hat{\mathbf{v}}^{(2)}\end{bmatrix}. \tag{A 3}$$

(*d*) Form a solenoidal, random, complex 3-vector with given helicity:

$$\hat{\mathbf{u}} = \hat{\mathbf{u}}^{(1)} + i(\mathbf{n}\times\hat{\mathbf{u}}^{(2)})/n. \tag{A 4}$$

Then the relative kinetic helicity is:†

$$\eta_V(k,0) = (\hat{\mathbf{u}}.\hat{\boldsymbol{\omega}}^*)/\langle\hat{\mathbf{u}}.\hat{\mathbf{u}}^*\rangle^{\frac{1}{2}}\langle\hat{\boldsymbol{\omega}}.\hat{\boldsymbol{\omega}}^*\rangle^{\frac{1}{2}} = \sin 2\theta, \tag{A 5}$$

where $\hat{\boldsymbol{\omega}} = i(\mathbf{k}\times\hat{\mathbf{u}})$. Also,

$$\hat{E}_V(k,0) = 8n^2C^2(n)S(n), \tag{A 6}$$

where $S(n)$ is the number of points in shell n. Thus specifying $\eta_V(k,0)$ and $\hat{E}_V(k,0)$ determines the adjustable constants θ and C for use in (A 1)–(A 4). A similar algorithm is used for generating fields with a given magnetic helicity or cross-helicity.

† Acknowledgement is made to S. A. Orszag for suggesting this technique.

REFERENCES

Bullard, E. C. & Gellman, H. 1954 *Phil. Trans. Roy. Soc.* A **247**, 213.

Frisch, U., Pouquet, A., Léorat, J. & Mazure, A. 1975 *J. Fluid Mech.* **68**, 769.

Gubbins, D. 1974 *Rev. Geophys. Space Phys.* **12**, 137.

Herring, J. R., Orszag, S. A., Kraichnan, R. H. & Fox, D. G. 1974 *J. Fluid Mech.* **66**, 417.

Jepps, S. A. 1975 *J. Fluid Mech.* **67**, 625.

Kraichnan, R. H. 1958 *Phys. Rev.* **109**, 1407.

Kraichnan, R. H. 1965 *Phys. Fluids* **8**, 1385.

Kraichnan, R. H. 1973 *J. Fluid Mech.* **59**, 745.

Kraichnan, R. H. & Nagarajan, S. 1967 *Phys. Fluids* **10**, 859.

Kropachev, E. P. 1971*a* *Geomag. Aeron.* **11**, 585.

Kropachev, E. P. 1971*b* *Geomag. Aeron.* **11**, 737.

Léorat, J. 1975 Thèse d'Etat, Université de Paris VII.

Léorat, J., Frisch, U. & Pouquet, A. 1975 *Ann. New York Acad. Sci.* **257**, 173.

Leslie, D. C. 1973 *Developments in the Theory of Turbulence.* Oxford: Clarendon Press.

Malkus, W. V. R. & Proctor, M. R. E. 1975 *J. Fluid Mech.* **67**, 417.

Moffatt, H. K. 1970*a* *J. Fluid Mech.* **41**, 435.

Moffatt, H. K. 1970*b* *J. Fluid Mech.* **44**, 705.

Moffatt, H. K. 1972 *J. Fluid Mech.* **53**, 385.

Moss, D. J. 1970 *Mon. Not. Roy. Acad. Sci.* **148**, 173.

Nagarajan, S. 1971 *IAU Symp. no.* 43, p. 487. Paris.

Orszag, S. A. 1970 *J. Fluid Mech.* **41**, 363.

Orszag, S. A. & Patterson, G. S. 1972 *Phys. Rev. Lett.* **28**, 76.

Parker, E. N. 1969 *Astrophys. J.* **157**, 1129.

Patterson, G. S. 1973 *11th Symp. Adv. Prob. Meth. in Fluid Mech., IPPT, Polish Acad. Sci.* p. 58.

Patterson, G. S. & Orszag, S. A. 1971 *Phys. Fluids* **14**, 2538.

Pouquet, A., Frisch, U. & Léorat, J. 1976 *J. Fluid Mech.* **77**, 321.

Roberts, P. H. 1967 *An Introduction to Magnetohydrodynamics.* Elsevier.

ROBERTS, P. H. & STIX, M. 1971 Translation of a series of articles by Steenbeck, Krause & Rädler. *Nat. Center Atmos. Res., Boulder, Colorado Tech. Note* IA-60.

RÜDIGER, G. 1973 *Astr. Nachr.* **294**, 183.

SCHUMANN, U. 1975 *12th Symp. Adv. Prob. Meth. in Fluid Mech., IPPT, Polish Acad. Sci.* (Also submitted to *Nucl. Eng. Des.*)

STEENBECK, M., KRAUSE, F. & RÄDLER, K. H. 1966 *Z. Naturf.* **21***a*, 369 (trans. by Roberts & Stix).

STEVENSON, A. F. & WOLFSON, S. J. 1966 *J. Geophys. Res.* **71**, 4446.

STIX, M. 1972 *Astron. Astrophys.* **20**, 9.

THOMAS, J. H. 1968 *Phys. Fluids* **11**, 1245.

VAINSHTEIN, S. I. 1974 *Sov. Phys., J. Exp. Theor. Phys.* **38**, 270.

VAINSHTEIN, L. L. & VAINSHTEIN, S. I. 1973 *Geomag. Aeron.* **13**, 123 (English trans.).

VAINSHSTEIN, S. I. & ZELDOVICH, Y. B. 1972 *Sov. Phys. Uspekhi* **15**, 159.

WEISS, N. O. 1966 *Proc. Roy. Soc.* A **293**, 310.

WILKINSON, A. & SMITH, F. G. 1976 *Mon. Not. Roy. Acad. Sci.* **167**, 593.